J Electroceram (2012) 28:80–87
DOI 10.1007/s10832-012-9683-x

Structural and electrical properties of $Sr(Ti, Fe)O_{3-\delta}$ materials for SOFC cathodes

Sebastian Molin · Weronika Lewandowska-Iwaniak · Boguslaw Kusz · Maria Gazda · Piotr Jasinski

Received: 3 July 2010 / Accepted: 13 January 2012 / Published online: 22 January 2012

Abstract Doped strontium titanates are very versatile materials. Iron doped $SrTiO_3$ can be used, for example, as a material for resistive gas sensors and fuel cell electrodes. In this paper, two compositions based on Fe doped $SrTiO_3$ were studied as possible candidates for cathode application in SOFCs. Namely, $SrTi_{0.65}Fe_{0.35}O_3$ and $SrTi_{0.50}Fe_{0.50}O_3$ were examined. A chemical reactivity between electrode and YSZ electrolyte material was investigated, since Sr containing cathode materials in contact with YSZ electrolyte are prone to form insulating phases. Electrical conductivity of bulk samples showed relatively low total conductivities of 0.4 S cm^{-1} and ~2 S cm^{-1} for STF35 and STF50 respectively. Suitability for cathode application was studied by Electrochemical Impedance Spectroscopy in a symmetrical electrode configuration. Area specific resistance (ASR) was determined in the temperature range from 600°C to 800°C. At 790°C samples show polarization ASR of approximately 0.1 Ω cm^2. It can be expected that further reduction of electrode ASR can be obtained by introduction of ceria barrier layer and tailoring of the electrode microstructure.

Keywords SOFC · Cathode · Impedance spectroscopy · Symmetrical electrodes · Strontium titanate

S. Molin (✉) · P. Jasinski
Faculty of Electronics, Telecommunications and Informatics,
Gdansk University of Technology,
Gdansk, Poland
e-mail: molin@biomed.eti.pg.gda.pl

W. Lewandowska-Iwaniak · B. Kusz · M. Gazda
Faculty of Applied Physics and Mathematics,
Gdansk University of Technology,
Gdansk, Poland

1 Introduction

Solid Oxide Fuel Cells (SOFCs) are solid-state energy conversion devices, which have recently attracted much attention [1]. Their main advantages are high efficiencies of energy conversion and broad range of fuels that can be used. Due to the operation at elevated temperatures high electrode activities can be achieved without the use of expensive precious metal catalysts. It is current research trend to lower the operating temperature of SOFC to the intermediate temperature range, i.e. 600°C–800°C. At lower temperatures cheaper materials might be used for SOFC fabrication. On the other hand, due to thermal activation mechanisms, the electrochemical performance of electrolyte and electrodes is reduced and thus new materials/technologies must be developed. In case of the electrolyte, which at lower temperatures suffers from an increase of ohmic resistance, an application of a thinner electrolyte provides a compensation for lowering temperature [2]. In case of the electrodes, the electrochemical performance is lowered due to rather sluggish chemical kinetics (chemical resistance) of oxygen reduction reaction (ORR), surface exchange kinetics, etc. [3]. This cannot be easily overcome by lowering thickness and new materials are sought.

Nowadays, SOFCs cathodes are almost exclusively fabricated using a perovskite family of materials [4]. The family is recognized by a general chemical formula of ABO_3. It can be substituted either in A or B site what results in alteration of perovskite physicochemical properties. For many years a $(La,Sr)MnO_3$ (LSM) cathode have gained broad popularity [5]. However, it is well documented that its main drawback is related to primarily electronic nature of conductivity and high activation energy for oxygen reduction reaction [6, 7]. It must be mixed with a good ionic conductor to form a mixed conducting electrode, which can

provide higher electrochemical performance. To simplify construction and achieve better results, alternative single phase MIEC (mixed ionic electronic conductors) electrode materials are sought.

One of the possible alternatives can be a member of the strontium titanate (STO) family. The STO has a perovskite crystal structure and can be easily doped. It is stable at high temperatures and has been extensively studied due to its good dielectric properties. In the undoped state, it has rather low conductivity and is a wide-bandgap semiconductor with E_g=3.2 eV at 0 K [8, 9]. It can be either acceptor or donor doped to meet many possible demands. For example, Nb doped STO has been presented as a successful resistive oxygen gas sensor [10]. In solid oxide fuel cells this material can be used for an anode fabrication. Nb doped STO with small additions of electrocatalytically active phase (Ni) has shown very good electrochemical performance when compared to the standard anode material of choice, i.e. the Ni-YSZ cermet [11, 12].

Iron doped strontium titanates, $SrTi_{1-x}Fe_xO_{3\pm\delta}$ (STF), present promising properties for resistive-type oxygen gas sensors [13, 14]. Due to their close to zero temperature coefficient of resistance (TCR) the STF materials are proposed as next generation oxygen sensors for exhaust gas monitoring in cars. Also, this material was successfully used for construction of propane gas sensor operating below 500°C [15]. The electrical properties of this material, including ratio of electronic/ionic conductivity (transference number), can be tuned by the doping level [16]. Recently, this material was used by Jung et al. [17] as a model mixed conductor dense cathode material for SOFC applications. Electrical conductivities in reducing and oxidizing atmospheres and chemical interactions with YSZ were studied before by Fagg et al. [18]. However, information about their electrocatalytic (oxygen reduction reaction) properties in symmetrical cells was not reported for porous samples.

The electronic conductivity of STF materials is rather low. For example, at the temperature 800ºC electronic conductivity of LSCF is as high as ~300 S cm^{-1}, while that of STF50 is only ~2 S cm^{-1} (Table 1). However, the chemical surface exchange coefficient and ionic conductivities of STF are higher than for other cathode candidates [17]. State of the art $(Ba,Sr)(Co,Fe)O_3$ perovskite has still better properties, but it is prone to detrimental reaction with CO_2 so that its broader use is not possible. The ionic conductivity of STF35 and STF50 is comparable to the ionic conductivity of YSZ electrolyte at 800°C (~0.035 S cm^{-1}). These potentially interesting properties have drawn attention to broader studies of these materials [17, 19].

The drawback of STF materials, as is also the case with many other perovskite cathodes, is their thermal expansion coefficient (TEC) that is higher than that of YSZ. For example, the TEC for $Sr_{0.97}Ti_{0.60}Fe_{0.40}O_3$ in the temperature range 720 K–1070 K is 16.6 ppm K^{-1} [20], while for YSZ approximately 10 ppm K^{-1}. The TEC of STF tends to increase with an increase in iron content.

Table 1 The electrochemical and electrical properties of selected perovskites. Data taken from [17]. Values given for 800°C

Material	Surface exchange coefficient	σ_{el}	σ_{ion}	t_{el}
–	cm s^{-1}	S cm^{-1}	S cm^{-1}	–
STF5	1.2×10^{-5}	4.5×10^{-3}	5.7×10^{-4}	0.88
STF10	1.4×10^{-5}	1.4×10^{-2}	1.7×10^{-3}	0.89
STF35	2.0×10^{-5}	9.9×10^{-1}	3.5×10^{-2}	0.96
STF50	1.7×10^{-5}	1.8	3.6×10^{-2}	0.97
LSCF	5.6×10^{-6}	3.0×10^{2}	8.0×10^{-3}	0.99

In this paper the preliminary study of $Sr(Ti,Fe)O_3$ materials as the potential porous SOFC cathode candidate are presented. Two different compositions are evaluated with respect to the Area Specific Resistance and the chemical interaction with the YSZ electrolyte.

2 Experimental

$Sr(Ti,Fe)O_{3-d}$ was prepared by a solid state reaction method. Dried powders of TiO_2, $SrCO_3$ and Fe_2O_3 (Aldrich, USA) were used as starting reagents. Two compositions were prepared: $SrTi_{0.65}Fe_{0.35}O_{3-d}$ (STF35) and $SrTi_{0.50}Fe_{0.50}O_{3-d}$ (STF50). Appropriate amounts of powders were milled in ethanol for 10 h in a zirconia ball mill (Fritsch 7, Germany) using ZrO_2 balls. Then they were compacted into pellets and calcined at 1100°C for 10 h. The pellets were re-ground, compacted and calcined for the second time at 1200°C for 15 h. Resulting powders were ball milled and used for the preparation of pastes and pellets. A commercial vehicle system was used for this purpose (ESL403, Electro-Science Laboratories, USA).

Bulk samples in the form of pellets were used for electrical conductivity measurements in a van der Pauw configuration. For this purpose the powders were compacted at 100 MPa and sintered at 1400°C for 4 h. Porosity of pellets (diameter ~13 mm, thickness ~2 mm) was ~8%. Silver (DuPont 4922 N, USA) electrodes were painted on the outer side of circular STF pellets and fired in-situ during heating of a tube furnace. Maximum silver current collector processing temperature was ~800°C and at that temperature it remained stable for the relatively short measurement time (several hours). DC resistance measurements were collected in stationary air using Keithley 2400 sourcemeter.

Area Specific Resistance (ASR) was measured in a symmetrical electrode configuration. Dense yttria stabilized zirconia (YSZ) pellets served as a substrate. A commercial

Tosoh 8YSZ powder was used to prepare dense electrolytes. YSZ powders were pressed at 150 MPa and sintered at 1400°C for 4 h in air. Porosities of electrolyte pellets (diameter ~12 mm, thickness ~800 μm) were lower than 4%. The STF paste was applied on both sides of electrolyte by brush painting. Mass change of samples during painting was controlled in order to get similar electrode thickness for all samples. After painting samples were left for 15 minutes at room temperature to level the paste and then were dried at 80°C. Afterwards samples were sintered at 1000/1100/1200°C for 1 h with heating and cooling rates of 3 °/min. Electrode diameter was approximately 10 mm. Electrodes, which were sintered at lower temperatures than 1000°C, suffered from delamination from YSZ and thus are not presented here. Initially, together with STF35 and STF50, also STF65 composition was investigated, but due to its high TEC it was impossible to fabricate well-adhered and reproducible STF65 layers on YSZ electrolytes.

After sintering, samples were placed in a spring loaded 4-wire cell with platinum meshes in contact with Ag current collector layer painted on top of STF electrodes. Impedance spectroscopy measurements were performed using Solartron 1260 frequency response analyzer. An amplitude of the excitation voltage of 25 mV was applied, frequency was altered from 1 MHz to 0.1 Hz. Spectra were collected starting from 800°C down to 600°C with 50°C intervals. The measurements were performed every 60 min to allow the system to equilibrate. Temperature control thermocouple was placed next to the sample in a distance of <2 mm.

The chemical reactivity tests of YSZ-STF composites were performed on 50:50 vol.% ratio powder mixtures. The mixtures were pressed into pellets at 50 MPa and fired in the same conditions as symmetrical electrodes (1000/1100/1200°C for 1 h). Additionally, chemical reactivity of compounds was checked by extended calcination (150 h) of those pellets at 800°C. The pellets were then ground in mortar to obtain powder for XRD phase analysis. Crystallographic structures and reaction products were checked using X-ray diffractometry. For these purposes a Philips X'Pert Pro diffractometer was used. XRD patterns were recorded with Cu K_α radiation at room temperature. Cross sectional and surface images were recorded using FEI-Philips XL30 ESEM scanning electron microscope.

3 Results and discussion

Temperature dependence of electrical conductivity of STF35 and STF50 pellets are shown in Fig. 1. It can be seen that the materials differ both in the value of conductivity and in its temperature dependence. The conductivity of STF35 and STF50 at 800°C is ~0.4 S cm^{-1} and ~2 S cm^{-1}, respectively. For lower iron content, x=0.35, conductivity

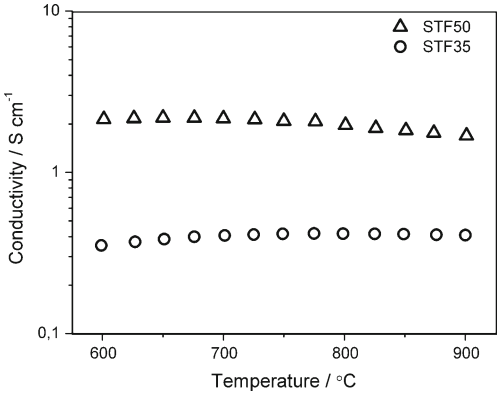

Fig. 1 Temperature dependence of DC electrical conductivity of STF35 and STF50 bulk samples

below 700°C increases when the temperature increase while it is almost constant in the range from 720°C up to 900°C. For higher iron content, conductivity decreases with the temperature increase. It agrees well with the previously reported results [13, 14, 21, 22]. As a general trend, at lower doping levels the conductivities increase with an increase of the temperature, while at higher temperatures the conductivities decrease with an increase of temperature. The sample close to the transition in the temperature behavior of conductivity shows a zero-TCR behavior. Indeed, as shown in the literature [13], the transition in temperature behavior is observed at iron doping level of x=0.35. Extensive information about these interesting properties is given in [14].

Electrical conductivities of both materials are low. The results obtained in this study are comparable to that reported in the literature [17]. The differences might be due to different porosities, differences in powder preparation procedure or different grain sizes. Conductivities reported here were obtained for almost dense samples. In case of the porous samples, values might be even one order of magnitude lower. Low electronic conductivity of material together with inefficient current collector on top of the electrode can result in an increase of constriction resistance [23]. On the other hand, reported properties (electrode polarizations surface exchange kinetics) of STF thin film cathodes were excellent, which makes the study of porous cathodes of interest for evaluation [17].

SEM images of STF50 electrode processed at 1200°C for 1 h are shown in Fig. 2(a) and (b). Figure 2(a) shows the surface of the electrode, while Fig. 2(b) the cross section of the sample. In the cross section image, the ~3 μm thick Ag current collector is visible on the top of the porous electrode. As can be seen in both images, the STF layer is highly porous, with average pore diameter of about 1–2 μm. The cathode particles are of about the same order of size. The thickness of the electrode is approximately 25 μm. Moreover, a ~3 μm thick dense interlayer is visible between the electrolyte and cathode. This is a product of the reaction of

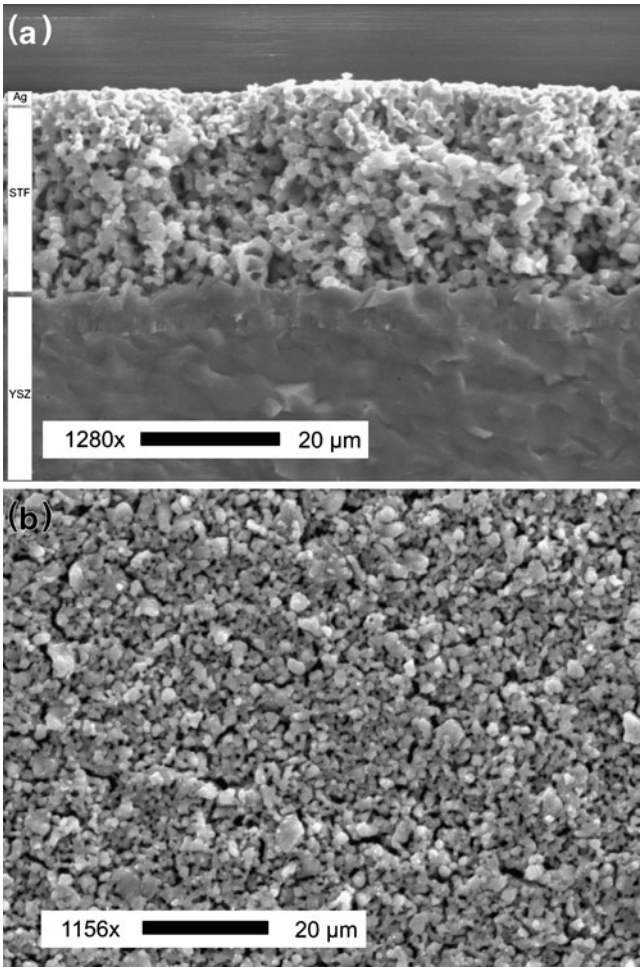

Fig. 2 (**a**) and (**b**). Scanning Electron Microscopy image of (**a**) the surface and (**b**) the cross section of STF50 electrode sintered at 1200°C for 1 h

between the cathode and electrolyte. Similar reaction product was observed in case of the $Sr_{0.97}Ti_{0.60}Fe_{0.40}O_3$ fired at 1350°C for 12 h [18]. The EDX analysis revealed that the reaction products are composed mainly of Sr and Zr, which form insulating $SrZrO_3$ [18].

Impedance spectra of symmetrical Ag/STF50/YSZ/STF50/Ag structures measured in the temperature range from ~600°C to ~800°C are presented in Fig. 3. In the insert, the spectra collected at 790°C are shown. At 790°C only one semicircle is distinguishable, while at 600°C at least two semicircles can be distinguished. The higher frequency semicircle has much lower resistance, while the resistance of lower frequency semicircle dominates. At 740°C and 790°C no distinction between these two can be made, which implies that the activation energy of the higher frequency semicircle is higher. In case of the dense STF, which was studied by Jung et al. [17], which were comparable in compositions to ones studied here, only one almost ideal semicircle was recorded. Authors concluded that the performance of thin, dense STF was limited by surface exchange kinetics. In this study layers were prepared by pulsed laser deposition with different thicknesses and surface areas, while the measurements were performed at different temperatures and different oxygen partial pressures. Those experimental conditions allowed for the determination of the rate determining reactions.

An ohmic resistance is defined as a high frequency x-axis intercept, while the polarisation resistance as a difference between low and high frequency intercepts, what can be described by the following formulas:

$$R_{ohmic} = R_{high\_frequency}[\Omega]$$
$$R_{polarization} = R_{low\_frequency} - R_{high\_frequency}[\Omega]$$

Although, at some temperatures the polarization part of the impedance is complex in shape, it is regarded in this study as only one resistance and no attempts are made to deconvolute its complex shape into possible sub-processes. To describe and compare electrode processes the Area Specific Resistance (ASR) is extensively used in the literature and in case of the symmetrical cells is defined as:

$$ASR = A\frac{R}{2}\left[\Omega\ \mathrm{cm}^2\right],$$

where R is the resistance, A is the electrode area and the factor of 2 in the denominator is related to two identical interfaces between electrolyte and electrode. Both ohmic and polarization resistances were used for calculation of $ASR_{ohmic/polarization}$, but factor of 2 is used only for calculation of the polarization ASR. Ohmic part of the impedance is attributed to electrolyte lossess, whereas polarization ASR is attributed to the complex electrode properties. Therefore ASR_{ohmic} is determined by the ohmic loss of the electrolyte and reaction product layer (between electrolyte and electrode) and $ASR_{polarization}$ is determined by STF material properties and

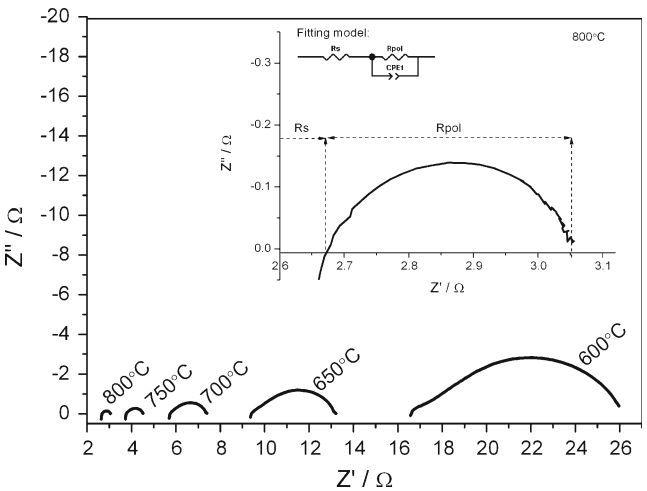

Fig. 3 Typical impedance spectra of STF50/YSZ/STF50 symmetrical electrode measured in the temperature range from 600°C to 800°C

possible interface electrochemical reactions. To determine electrode performance $ASR_{polarization}$ values are compared and evaluated.

The temperature dependence of ohmic ASR is shown in Fig. 4. The ASR values at 790°C are also presented in Table 2. The values of ohmic ASRs are very similar for all samples, i.e. they weakly depend on the processing temperature (see Table 2). ASR values obtained for STF50 are lower than that for STF35, which might be explained by higher electronic conductivity of the former material. The thickness of the YSZ electrolyte pellet was ~0.8 mm, which should result in ASR resistance of approximately 2.2 Ωcm^2 (calculated for σ_{YSZ}=0.035 S cm^{-1} at 800°C). This is in agreement with values obtained for the ohmic ASR reported here. The activation energies of ohmic ASR are about 0.72 eV, what is lower than for pure YSZ (expected E_a ~1 eV). This can indicate influence of the STF layer on the ohmic resistance. As is shown in Fig. 2(b), reaction products are present at the interface of the electrolyte and electrode, forming low conductivity $SrZrO_3$ layer. However, the increase of the sintering temperature is not manifested by the increase of ohmic ASR. It suggests that other parameter must be responsible for the ohmic resistance. It can be the ohmic drop through the cathode or constriction resistance due to current collection from weakly conductive electrode.

The polarization ASR values for STF35 and STF50 are shown in Fig. 5. In this case the sintering temperatures have a strong influence on the electrochemical behavior. The electrodes sintered at 1200°C have more than an order of magnitude higher ASR than that sintered at 1000°C. In the case of the electrodes sintered at 1200°C and 1000°C similar ASR polarization resistance are obtained for STF35 and STF50, at 1100°C significant difference is observed. As was observed by Mai et al. [24], reaction between YSZ and Sr containing cathode leads to increase in both the serial and polarization resistance, from which the latter one is dominant. The change in the polarization ASR can be connected to formation of $SrZrO_3$ perovskite phase with poor oxygen ion conductivity (4.3×10^{-5} S cm^{-1} at 750°C [25]). The lowest ASR polarization resistances of 0.124 Ω cm^2 and 0.143 Ω cm^2, for STF35 and STF50 respectively, were obtained at ~790°C for the electrodes sintered at 1000°C. The higher level of electrical conductivity of STF50 (~5 times) is not clearly manifested on ASR polarization resistances. The ASR activation energies were in the range of 1.20–1.36 eV with slightly lower values for STF50 compositions. Those activation energies are in the range usually reported for other cathode materials, e.g. in the case of the LSM [5] or (La,Sr)(Co,Fe)O_3-(Ce,Sm)O_2 (LSCF-CSO) composites (1.2 eV–2 eV) [26]. The results of polarization resistances for STF mixed conductor cathode are between pure electronic conductors like LSM and mixed conductors based on composites, e.g. LSCF-(Ce,Gd)O_2 system [27] or state-of-the-art (Ba,Sr)(Co,Fe)O_3 (BSCF) [28]. For pure LSM on YSZ an ASR of 3.5 Ωcm^2 at 750ºC was obtained [29], while for LSCF on YSZ an ASR of ~0.1 Ωcm^2 was obtained at the same temperature [30]. The mechanism of the rate limiting step is to be examined in further studies, however it is rather unlikely, that surface exchange kinetics will be the limiting factor for porous mixed conducting electrodes [31]. At this stage it is not possible to evaluate the effects of sintering for electrodes prepared at higher temperatures, since the results are dominated by the reaction between STF and YSZ. Sintering leads to increase in grain contact on one hand but on the other hand leads to lower porosity, so that existence of an optimum sintering temperature is expected [32] and will be studied in the future.

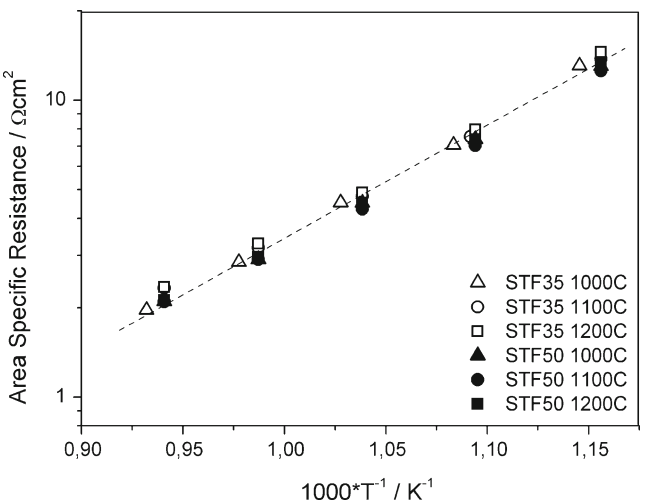

Fig. 4 Ohmic Area Specific Resistance for the STF35 and STF50 samples versus inverted temperature

The obtained ASR polarization resistance results are encouraging for further studies of STF for SOFC application. It is impossible to compare them directly with other reports, since similar data are not available for the porous STF cathodes in symmetric electrode or SOFC configuration. The data obtained for thin dense electrodes are not easily comparable. Jung et al. [17] have shown that the ASRs of STF35 and STF50 were approximately of 2–3 Ω cm^2 at 650°C. There was a tendency to lower ASR with an increase of iron content, however for iron content above 0.35 the increase become insignificant. The introduction of porosity into a cathode structure, in this study, lowers its electrical conductivity and provides access for oxygen at electrochemically active sites. As the result of much higher surface area for oxygen exchange, the effect of rate determining surface exchange kinetics can be limited. Canales-Vazquez et al. [33] studied Fe substituted $La_{0.33}Sr_{0.67}Ti_{1-x}Fe_xO_3$ (LSTF). In symmetrical configuration the ASR polarization of ~0.5 Ω cm^2 was obtained at 900°C for the electrodes with $x_{(Fe)}$=0.50. It should be stressed, that results reported in this study are comparable to

Table 2 Comparison of electrical properties of STF35 and STF50 sintered at different temperatures

Sample:	Sintering temperature	Ohmic E_a [eV]:	Ohmic ASR ~790°C [Ωcm^2]	Polarization E_a [eV]:	Polarization ASR ~790°C [Ωcm^2]
STF35	1000°C	0.74	2.28	1.28	0.12
	1100°C	0.69	2.33	1.27	0.76
	1200°C	0.70	2.35	1.35	4.61
STF50	1000°C	0.71	2.10	1.25	0.14
	1100°C	0.69	2.10	1.23	0.29
	1200°C	0.71	2.12	1.29	3.71

results obtained on porous LSCF cathodes [34–36], LNF cathode [37] and LSM-YSZ composites [38]. All of these materials exhibit much higher electronic conductivities, so results obtained for STFs are interesting. It can be expected that the enhancement of the STF microstructure and mitigation of formation of insulating phases, may improve the ASR polarization.

The chemical reaction between STF35/STF50 and YSZ was investigated using XRD analysis of YSZ and STF composite powders (50/50 vol% mixtures) annealed in different conditions. Both studied powders provided similar results and thus only patterns of the reacted STF35 are presented here (Fig. 6). The XRD reflexes observed in the patterns correspond to YSZ, STF and their reaction products. Reaction products are present for all studied sintering temperatures. With an increase of the sintering temperature, the intensity of peaks originating from STF perovskite phase (2θ=32.3°, 46.5°, 57.8°) decreases due to the formation of $SrZrO_3$ based compounds. With an increase of the processing temperature, the reaction products peak detected initially at 2θ=31.0° shifts to 2θ=31.35° with a simultaneous increase of its intensity (inset in Fig. 6). At 1100°C additional peak at 2θ=32.0° is detected, which at 1200°C does not change its position, but increases intensity and become more prominent than the peak at 2θ=31.35°. Peak shifting to higher 2θ values suggest a decrease of cell parameter. Ionic radii of reacting species: Fe^{IV+}=0.585 Å, Ti^{IV+}=0.605 Å, are smaller than ionic radii of Zr^{IV+}=0.72 Å. Forming $SrZrO_3$ based phases can probably substitute Fe, Ti into B site, what results in a change of cell dimensions. Also some Zr can be incorporated into STF lattice changing its properties. Probably these two mechanisms occur simultaneously and are responsible for two perovskite reaction products. Intensity of the peaks corresponding to the reaction products is the highest for the sintering temperature of 1200°C, where STF originating peaks are diminished in intensity. Fagg et al. [18] reported that after 10 h at 1350°C, a mixture of YSZ and STF was almost fully reacted. At lower temperatures they also detected forms of $SrZrO_3$ based oxides.

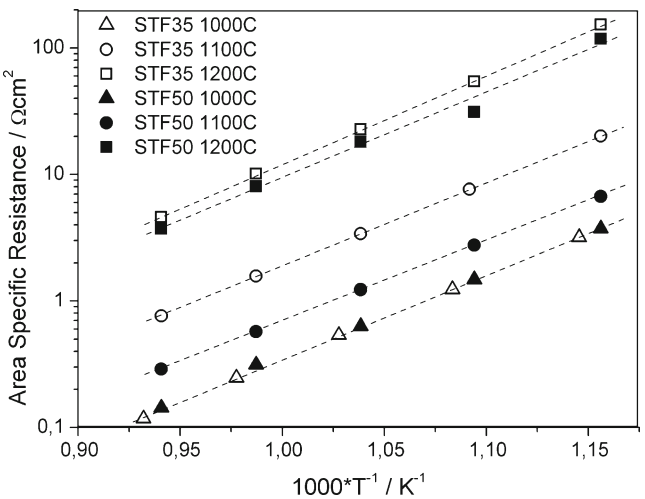

Fig. 5 Temperature dependence of polarization Area Specific Resistance for STF35 and STF50 samples

The reactivity studies of YSZ and STF were also carried out by isothermal treatment of STF-YSZ powder mixtures at 800°C for 150 h. This is an operating temperature of intermediate temperature SOFCs and the aging behavior is of primary importance. In this case the mixtures were not calcined at higher temperatures. After 150 h of isothermal treatment a small peak corresponding to the reaction products is visible. This is the same phase as observed for higher calcination temperatures. The same phenomena occur for all Sr (and La) containing materials and it can be avoided by application of doped ceria interlayer on YSZ electrolyte, which is much less reactive with cathode powders and acts as a barrier layer. The dense STF cathode behavior studied by Jung et al. [17] included measurement of the electrode behavior on YSZ and, as a reference, on a CGO. No noticeable differences in ASRs were obtained, implying that the cathode electrochemical processes were limiting. In their case, however, the samples were deposited as thin films by a pulsed laser deposition (PLD) method, so temperature treatment was avoided. The maximum studied temperature was 650°C. Cathodes processed at high temperature (>1000°C) usually heavily react with the YSZ electrolyte, what significantly increases electrode resistance. The incorporation of ceria barrier layer between the cathode and electrolyte lowers the reaction extend and in effect the electrode resistance should be lowered. The electrode

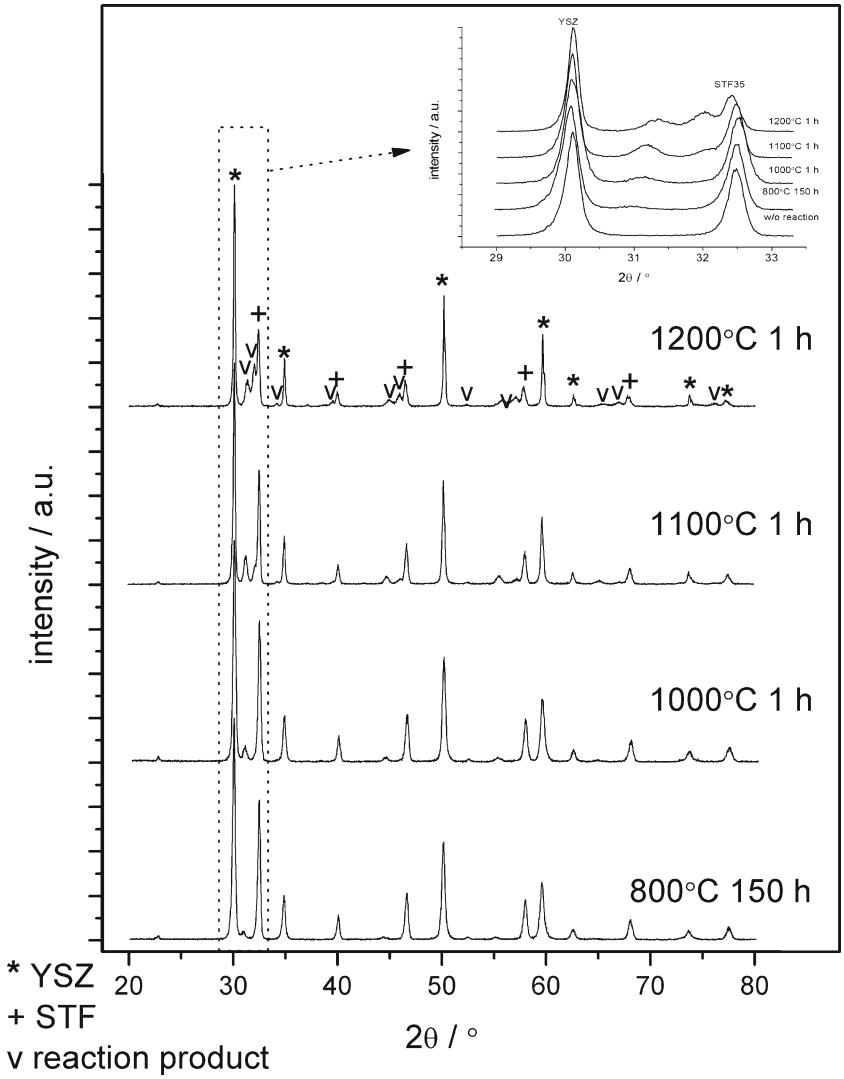

Fig. 6 X-ray diffractometry study of 50:50 vol.% mixtures of YSZ and STF35 annealed in different conditions

properties obtained in this study are very encouraging and further studies adopting ceria buffer layer between cathode and electrolyte are planned.

4 Conclusions

In this paper the electrical properties and reactivity with YSZ of $SrTi_{0.65}Fe_{0.35}O_3$ and $SrTi_{0.50}Fe_{0.50}O_3$ were investigated with respect to potential SOFC cathode application. For the first time porous STF electrodes in a symmetrical configuration were investigated and these results are reported here. The best results are obtained for STF electrodes sintered at 1000°C. Namely, the polarization ASRs of ~0.1 Ω cm^2 at ~790°C and activation energies of ~1.3 eV were obtained. The ASR polarization resistances were strongly affected by the sintering temperature, while the ASR ohmic resistances were not sensitive to this parameter. The higher electrical conductivity of STF50 composition in comparison to STF35 did not lead to the improved cathode performance. Relatively low electronic conductivities combined with high ionic conductivities results in good overall performance as possible SOFC cathodes. It is expected that tailoring STF microstructure can lower ASR resistances, similar to other cathode materials. Reactivity studies show that sintering at 1000°C, 1100°C and 1200°C and long-term operation at 800°C results in formation of $SrZrO_3$ based phases. This study shows, as the complement to previous results obtained for dense STF thin films, the feasibility for use of porous STF cathodes as oxygen reduction electrodes for SOFCs. Future studies will include the study of the influence of CGO barrier layers and will focus on microstructure optimization, which should improve cathode parameters.

Acknowledgment This work has been supported by a grant from Polish Ministry of Science and Higher Education "N N511 376135".

S. Molin also wishes to thank the Marshal of the Pomorskie Voivodeship for the "InnoDoktorant - Scholarships for PhD students, II edition" and for Foundation for Polish Science START 2011 stipend for young researchers.

References

1. M. Dokiya, Solid State Ionics **152**, 383–392 (2002)
2. J. Will, A. Mitterdorfer, C. Kleinlogel, D. Perednis, L.J. Gauckler, Solid State Ionics **131**, 79–86 (2000)
3. S.B. Adler, Chem. Rev. **104**, 4791–4843 (2004)
4. A.J. Jacobson, Chem. Mater. **22**, 660–674 (2010)
5. S. Jiang, J. Mater. Sci. **43**, 6799–6838 (2008)
6. Y. Li, R. Gemmen, X. Liu, J Power Sources **195**, 3345–3358 (2010)
7. C. Sun, R. Hui, J. Roller, J. Solid State Electrochem. **14**, 1125–1144 (2010)
8. G.M. Choi, H.L. Tuller, D. Goldschmidt, Phys. Rev. B **34**, 6972–6979 (1986)
9. R. Meyer, R. Waser, Sensors Actuators B Chem **101**, 335–345 (2004)
10. J. Abrantes, J.A. Labrincha, J.R. Frade, Sensors Actuators B Chem **56**, 198–205 (1999)
11. P. Blennow, K.K. Hansen, L.R. Wallenberg, M. Mogensen, Solid State Ionics **180**, 63–70 (2009)
12. J. Karczewski, B. Riegel, S. Molin, A. Winiarski, M. Gazda, P. Jasinski, L. Murawski, B. Kusz, J Alloy Compd **473**, 496–499 (2009)
13. R. Moos, F. Rettig, A. Hürland, C. Plog, Sensors Actuators B Chem **93**, 43–50 (2003)
14. A. Rothschild, S.J. Litzelman, H.L. Tuller, W. Menesklou, T. Schneider, E. Ivers-Tiffée, Sensors Actuators B Chem **108**, 223–230 (2005)
15. K. Sahner, R. Moos, M. Matam, J.J. Tunney, M. Post, Sensors Actuators B Chem **108**, 102–112 (2005)
16. R. Moos, K.-H. Hardtl, J. Am. Ceram. Soc. **80**, 2549–2562 (1997)
17. W. Jung, H.L. Tuller, Solid State Ionics **180**, 843–847 (2009)
18. D.P. Fagg, V.V. Kharton, J.R. Frade, A.A.L. Ferreira, Solid State Ionics **156**, 45–57 (2003)
19. C. Argirusis, F. Jomard, S.F. Wagner, W. Menesklou, E. Ivers-Tiffée, Solid State Ionics **192**, 9–11 (2010)
20. E. Bartonickova, K. Wiik, K. Maca, H.L. Lein, E.A. Rudberg, J. Eur. Ceram. Soc. **30**, 605–611 (2010)
21. G. Neri, A. Bonavita, G. Micali, G. Rizzo, R. Licheri, R. Orrù, G. Cao, Sensors Actuators B Chem **126**, 258–265 (2007)
22. A. Rothschild, W. Menesklou, H.L. Tuller, E. Ivers-Tiffee, Chem. Mater. **18**, 3651–3659 (2006)
23. E.V. Tsipis, V.V. Kharton, J. Solid State Electrochem. **12**, 1367–1391 (2008)
24. A. Mai, M. Becker, W. Assenmacher, F. Tietz, D. Hathiramani, E. Ivers-Tiffee, D. Stover, W. Mader, Solid State Ionics **177**, 1965–1968 (2006)
25. F.W. Poulsen, N. van der Puil, Solid State Ionics **53–56**, 777–783 (1992)
26. C.J. Fu, K.N. Sun, X.B. Chen, N.Q. Zhang, D.R. Zhou, Electrochim. Acta **54**, 7305–7312 (2009)
27. J.J. Bentzen, J.V.T. Hogh, R. Barford, A. Hagen, Fuel Cells **9**, 823–832 (2009)
28. W. Zhou, R. Ran, Z. Shao, J Power Sources **192**, 231–246 (2009)
29. E. Perry Murray, S.A. Barnett, Solid State Ionics **143**, 265–273 (2001)
30. E. Perry Murray, M.J. Sever, S.A. Barnett, Solid State Ionics **148**, 27–34 (2002)
31. S.B. Adler, Solid State Ionics **135**, 603–612 (2000)
32. M.J. Jørgensen, S. Primdahl, C. Bagger, M. Mogensen, Solid State Ionics **139**, 1–11 (2001)
33. J. Canales-Vázquez, J.C. Ruiz-Morales, D. Marrero-López, J. Pena-Martınez, P. Núnez, P. Gómez-Romero, J. Power Sources **171**, 552–557 (2007)
34. X. Lou, S. Wang, Z. Liu, L. Yang, M. Liu, Solid State Ionics **180**, 1285–1289 (2009)
35. C. Fu, K. Sun, N. Zhang, X. Chen, D. Zhou, Electrochim. Acta **52**, 4589–4594 (2007)
36. J. Chen, F. Liang, B. Chi, J. Pu, S.P. Jiang, L. Jian, J. Power Sources **194**, 275–280 (2009)
37. M. Bevilacqua, T. Montini, C. Tavagnacco, E. Fonda, P. Fornasiero, M. Graziani, Chem. Mater. **19**, 5926–5936 (2007)
38. T. Suzuki, M. Awano, P. Jasinski, V. Petrovsky, H.U. Anderson, Solid State Ionics **177**, 2071–2074 (2006)